# Forces on dislocations due to strain gradients: Theories and two-dimensional simulations

Paulo César N. Pereira [*] and Sérgio W. S. Apolinário [†]
*Departamento de Física, Universidade Federal de Pernambuco, 50670-901 Recife, PE, Brazil*

(Received 2 June 2022; accepted 21 June 2022; published 19 December 2022)

Dislocations are topological defects known to be crucial in the onset of plasticity and in many properties of crystals. Classical elasticity fails to fully explain their dynamics under extreme conditions of high gradients of strain and small scales, which can nowadays be scrutinized. Previous works have proposed a type of force acting on dislocations when they are in the presence of strain gradients, the so-called core force. Here we designed a two-dimensional atomistic simulation through which we confirm the existence of this force, probe its properties, and measure its coefficients. The results of our simulations agree with the assumption that the core energy is the origin for the core force, but the coefficients of this force cannot be predicted by the approaches previously proposed. We show that the measured coefficients can be used to obtain the core energy in some systems such as ours. This way of evaluating the core energy can be compared to other existing approaches. Moreover, we show that the core force implies the existence of nonreciprocal interactions between dislocations. We believe that a correct consideration of the core force can be considered in mechanical modeling and in some theories trying to explain strange phenomena in plasticity.

DOI: 10.1103/PhysRevB.106.224105

## I. INTRODUCTION

The idea of dislocation defects was first conceived mathematically [1] and later applied in the context of plasticity [2], by considering the movement of defects in a periodic lattice. It soon became a vital feature of investigation in real three-dimensional (3D) crystals [3–5]. Since the bubble-raft model [6], two-dimensional (2D) crystals have also been used as simple models to study dislocation dynamics (e.g., using colloids [7], complex plasmas [8], and vortices in superconductors [9]).

The individual dislocation movement is generally assumed to be governed by some well-known mechanisms: The Peach-Koehler (PK) driving force [10] and the Peierls-Nabarro barrier [11,12] aside from other possible motion's resistance, climb, and diffusion mechanisms [4,5,13,14]. These forces have been widely used to model plastic deformations in discrete dislocation dynamics (DDD) simulations [5,14], where the exact locations of all atoms can be ignored and one only needs to consider the dynamics of dislocation lines, in 3D, or points, in 2D. The validity of such mesoscale approach relies on the forces and mobility law that it considers.

The mechanisms cited above cannot fully explain the full range of new plastic phenomena with technological impact observed, e.g., in micron and submicron scales [15–19] (with a "smaller is stronger" trend) and during shock loadings [20–25]. These are situations where high gradients of strain and strain rates appear. As a consequence, several phenomenological and mechanism-based models have been developed, including corrections to the mobility law [26], nonlocal elasticity [27,28], and strain gradient plasticity [29–33].

Clouet [34] observed that the usual mathematical representation for the origin of the so-called core field leads to a fundamentally different type of driving force on a dislocation. It is a force proportional to the derivatives of the background strains, which are the ones generated by all sources of strain but the dislocation itself. Such type of force has been called the core force and can contribute, in a fundamental manner, for the emergence of strange phenomena when high gradients of strain are present. Clouet's theoretical framework predicted a relation between the coefficients of the core force and the ones of the core field.

Another approach for the core force was made by Iyer *et al.* [35], considering that the core force can be viewed as originated from the interaction of the core with the background strains. They developed an electronic-structure evaluation of the core energy, in its standard definition, for different background strains. They used this to predict the coefficients of the core force that can act on the dislocation. But they do not discuss about the ambiguity due to the arbitrariness of the core radius present in the standard core-energy definition.

The aim of our work is to broaden current knowledge about the core force. In spite of the previous theoretical works, such type of force has not been directly observed and identified, neither through simulations nor through experiments. It is usually much smaller than PK and to identify it one needs the precise knowledge of both the strains and the resulting force on a dislocation. To meet this requirement, we design, in this work, a 2D system where these variables are completely known. We simulate it, demonstrating the existence, probing the properties, and measuring the coefficients of the core force on edge dislocations.

By analyzing simulations and theories, we found that the current theoretical proposals for the core force are insufficient to explain or predict the results of our 2D simulations. This

[*] paulo.cesarpereira@ufpe.br
[†] sergio.apolinario@ufpe.br

 

is summarized in Sec. V C and shown in table. We observed that, e.g., Clouet's approach has quantitative problems and the one used by Iyer *et al.* is ill defined.

As another discovery, we observe that, in systems with scale invariance such as the one in our simulations, the core energy can be obtained directly from the core-force coefficients. A definite value for this quantity is obtained although the core energy is usually defined in an ambiguous manner. This unambiguous evaluation can be compared with other studies which need or predict the existence of a specific core energy with physical meaning, such as the Kosterlitz, Thouless, Halperin, Nelson, and Young (KTHNY) theory for 2D melting [36] and the Kanzaki force approach to represent crystalline defects [37].

The next section introduces some basic assumptions about the core force and lists its properties. Interesting remarks are made regarding interactions between dislocations, where size effects and nonreciprocal interactions that appear in the system. In Secs. III and IV, we present the setup and the results of our 2D simulations, respectively. Finally, in Sec. V, we compare the simulation results with the theoretical proposals.

## II. SOME ASSUMPTIONS ABOUT THE CORE FORCE

Our work investigates the core force through simulation and theory. By "core force" we mean the phenomenon of background strain or stress gradients being responsible for a driving force on dislocations. Before going further, we make some initial assumptions about this force and discuss some of their consequences. They are intuitive guesses that will be probed in the following sections, via simulations.

### A. Effective existence of the core force

Although previous works [34,35,38] have predicted the core force, a direct observation (i.e., via simulation or experiment) is needed in order to confirm its effective action. This is because such works did not investigate how the background strain gradients can affect barriers to movement (such as the Peierls-Nabarro or a possibly new one) which could, in principle, strengthen when in the presence of them.

In fact, it is known that the PN barrier is affected by the background strain [39,40]. Thus, if this barrier is also proportional to the background strain gradients, it can cancel out or just weaken the effective intensity of the core force. In our work, we performed simulations that can probe if the observed core force is effectively a driving one, i.e., capable of driving a dislocation.

### B. Driving-force definition and the separation between PK and core forces

The driving force on a dislocation $\mathbf{f}^{\text{disl}}$ is defined through

$$\delta E^{\text{disl}} = -\mathbf{f}^{\text{disl}} \cdot \delta \mathbf{r}^{d}, \tag{1}$$

where $\delta E^{\text{disl}}$ is the variation of the total dislocation energy when this defect moves by $\delta \mathbf{r}^{d}$. Classical elasticity evaluation of Eq. (1) leads to the so-called Peach-Koehler force $\mathbf{f}^{\text{PK}}$ [10]. We consider that the core force $\mathbf{f}^{\text{core}}$ is not a modification of the PK force, but another type of driving force to be added, such that the total driving force on the dislocation is

$$\mathbf{f}^{\text{disl}} = \mathbf{f}^{\text{PK}} + \mathbf{f}^{\text{core}}. \tag{2}$$

Moreover, while $\mathbf{f}^{\text{PK}}$ depends only on the background strains $\varepsilon_{ij}^{bg}$, we consider that $\mathbf{f}^{\text{core}}$ depends only on the derivatives (i.e., first gradients and possibly higher-order ones) of $\varepsilon_{ij}^{bg}$.

### C. Possible properties of the core force

Our simulations are done in the regime of small strains and small strain gradients. This allows us to probe some properties of the core force. We expect that, in this regime, it has the linearity property, i.e.,

$$\begin{aligned}\mathbf{f}^{\text{core}} &= \mathbf{f}^{\text{core}}\left(\nabla\varepsilon_{ij}^{bg}, \nabla\partial_k\varepsilon_{ij}^{bg}, \dots\right)\\ &= M_{ij}\nabla\varepsilon_{ij}^{bg} + M_{kij}\nabla\partial_k\varepsilon_{ij}^{bg} + \cdots,\end{aligned} \tag{3}$$

where we use the Einstein summation convention. Equation (3) is an intuitive guess about the core-force behavior. In this section, we list the main properties expected for the core force within this guess.

Within the regime of small deformations, the linearity property is *a priori* expected for the elasticity and plasticity phenomena. The core force would then be a linear response to the background strain gradients, i.e., linearly dependent on them. In fact, we expect that the core force is perturbatively well behaved.

We assume that the tensor coefficients ($M_{ij}$, $M_{kij}$, ...) are constants of the crystal, depending only on the glide direction. Thus, this force obeys the uniqueness property. In other words, the uniqueness means that $\mathbf{f}^{\text{core}}$ depends only on the present crystal configuration and not on its history. It does not depend on where the dislocation was before, for example.

The given core force is also symmetric under Burgers vector inversion. This is not the case for the PK force, which has an explicit dependence on the Burgers vector $\mathbf{b}$, given by [4,13]

$$\begin{aligned}\mathbf{f}^{\text{PK}} &= \mathbf{f}^{\text{PK}}\left(\varepsilon_{ij}^{bg}\right)\\ &= \boldsymbol{\sigma}^{bg} \cdot \mathbf{b} \times \hat{\mathbf{z}},\end{aligned} \tag{4}$$

where $\sigma_{ij}^{bg} = \sigma_{ij}^{bg}(\varepsilon_{ij}^{bg})$ is the background stress.

Finally, note that the derivatives in Eq. (3) are evaluated at the dislocation position. Thus, $\mathbf{f}^{\text{core}}$ satisfies the locality property. In other words, the force depends only on the crystal configuration very near the dislocation. This is expected if such force is indeed originated from the interaction between the background and the dislocation core structure.

### D. Summary of the properties to be probed by simulations

The previous assumptions are yet to be confirmed. In summary, atomistic simulations or experiments are needed in order to probe the following properties of the force: (i) effective driving action, i.e., the capability to move a dislocation through this force; (ii) linear dependence on the background strain derivatives; (iii) uniqueness; (iv) symmetry under Burgers vector inversion; (v) locality. The item (i) seems to be the most obvious one, but it still needs to be verified. In Sec. II A we comment about the importance of verifying it.

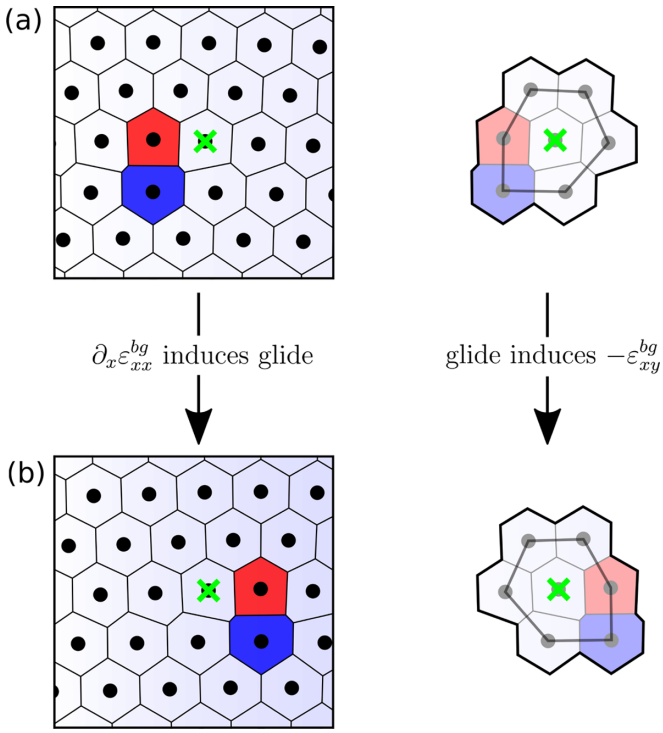


FIG. 1. Sequence of equilibrium configurations inside the same part of the system where we can see a dislocation that glided due to the action of the core force induced by $\partial_x \varepsilon_{xx}^{bg}$. On the right side of the figure, the neighborhood of the particle marked by a green cross is evidenced. In (a), the dislocation, represented by the particles with 5 (red) and 7 (blue) neighbors in the Voronoi tessellation, is in equilibrium. Here, a small PK force pointing to the left is counterbalanced by a core force pointing to the right. The light blue shown in the background illustrates the variation in $\varepsilon_{xx}^{bg}$, increasing in the right direction. (b) As we increase the strain gradient in the background of the dislocation position, the defect moves to the right, reaching a new position where the strain gradient is smaller and the core force equals PK again, and then it equilibrates. As we can see from the change in the region around the particle marked by a green cross, the dislocation glide induced a negative resolved shear deformation (i.e., $-\varepsilon_{xy}^{bg}$).

Our simulations presented in this paper have observed dislocations gliding due to strain gradient forces, as shown in Fig. 1, where all the properties (i)–(v) are satisfied. In Sec. V, we show how the confirmation of each of these properties can be used to discard some theoretical proposals for the core force.

### E. Consequences for dislocation interactions: Size effects and nonreciprocity

The force between dislocations can be obtained from the background strains that they induce on one another. For the classical linear elasticity theory, the leading contributions to the deformation fields induced by a dislocation are exactly solvable and are called the Volterra solutions [4,13]. Within such theory, the PK and core forces on a dislocation at $\mathbf{r}^\alpha$ due to another one at $\mathbf{r}^\beta$ behave as

$$\mathbf{f}^{\rm PK}_{\beta\to\alpha} \propto 1/|\mathbf{r}^\alpha - \mathbf{r}^\beta| \quad \text{and} \quad \mathbf{f}^{\rm core}_{\beta\to\alpha} \propto 1/|\mathbf{r}^\alpha - \mathbf{r}^\beta|^2, \tag{5}$$

respectively, where we considered the core force only up to first gradients. If we consider the PK force alone, the resulting power-law dynamics has no intrinsic length scale and obeys the so-called similitude principle, leading to a dislocation dynamics that is qualitatively independent of size.

With the additional consideration of $\mathbf{f}^{\rm core}$, the total interaction loses the single power-law character and an intrinsic length scale appears, leading to a fundamental origin of size effects. Another type of correction to the classical PK interaction which behaves similarly to the core force (i.e., with $\propto 1/|\mathbf{r}^\alpha - \mathbf{r}^\beta|^2$), but with a different angular dependence, is the PK force due to the core-field strain and has been investigated as a possible origin of size effects [41,42].

For the dislocation interactions in Eq. (5), an interesting analysis can be made for the case of a system with identical dislocations. In this case, we have

$$\mathbf{f}^{\rm PK}_{\beta\to\alpha} = -\mathbf{f}^{\rm PK}_{\alpha\to\beta} \quad \text{and} \quad \mathbf{f}^{\rm core}_{\beta\to\alpha} = \mathbf{f}^{\rm core}_{\alpha\to\beta}, \tag{6}$$

which are consequences of the Volterra strain property $\varepsilon^V_{ij}(\Delta\mathbf{r}) = -\varepsilon^V_{ij}(-\Delta\mathbf{r}) \Rightarrow \nabla\varepsilon^V_{ij}(\Delta\mathbf{r}) = \nabla\varepsilon^V_{ij}(-\Delta\mathbf{r})$. This means that the core force provides nonreciprocal interactions between the dislocations. It can be shown that the PK force due to the core-field strain also has this nonreciprocity. Such type of interaction violates Newton's third law and has been extensively studied recently [43–46]. When two "particles" interact like this, they can, e.g., drive each other indefinitely through the system, under some conditions.

## III. SIMULATION OF THE CORE FORCE

In this section, we discuss the theoretical motivations for the choice of our simulation model. In Sec. III A, the basic theoretical equations that we use are shown. These are the classical elasticity equations, which give well approximate predictions for the background strains in the regime of small deformations, and the proposed equation for the core force. In Sec. III B, we comment some precautions that, if taken, allow us to obtain good numerical precision in our investigations. Finally, in Sec. III C, we detail the simulation setup that we chose to use and comment its advantages. The results of the simulations are shown in the next section.

### A. Basic equations

When the particle positions in a crystal are displaced, i.e., $\mathbf{r} \to \mathbf{r} + \mathbf{u}(\mathbf{r})$, there is an energetic change due to the interparticles' interactions. In the 2D classical elasticity approximation, the elastic potential energy due to the displacement field $\mathbf{u}(\mathbf{r})$ in the presence of a body force density field $\mathbf{f}(\mathbf{r})$ is given by [13]

$$E^{el}[\mathbf{u}(\mathbf{r})] = \int \left[\frac{1}{2} C_{ijkl}\varepsilon_{ij}(\mathbf{r})\varepsilon_{kl}(\mathbf{r}) - f_i(\mathbf{r})u_i(\mathbf{r})\right] d^2r, \tag{7}$$

where $\varepsilon_{ij} = (\partial_i u_j + \partial_j u_i)/2$ are the strains. For the triangular lattice, the elastic constants are $C_{ijkl} = B\delta_{ij}\delta_{kl} + \mu(\delta_{ik}\delta_{jl} + \delta_{il}\delta_{jk} - \delta_{ij}\delta_{kl})$, where $B$ and $\mu$ are the bulk and shear moduli, respectively. The equilibrium condition $\delta E^{el}/\delta u_i = 0$ gives

$$C_{ijkl}\partial_j\partial_l u_k + f_i = 0 \tag{8}$$

and the stress-strain relation is $\sigma_{ij} = C_{ijkl}\varepsilon_{kl}$.

The Burgers vector $\mathbf{b}$ of a dislocation at $\mathbf{r}^d$ is defined as $\mathbf{b} = \oint d\mathbf{u}$, for small counterclockwise closed curves enclosing $\mathbf{r}^d$. For a dislocation with $\mathbf{b} = b\,\hat{\mathbf{x}}$ in a triangular crystal, the glide component (i.e., the $x$ component) of the driving force (2) on it is given by

$$f_x^{\text{disl}} = 2\mu b\varepsilon_{xy}^{bg} + M_{ij}\partial_x\varepsilon_{ij}^{bg} + M_{kij}\partial_x\partial_k\varepsilon_{ij}^{bg} + \cdots, \qquad (9)$$

where $f_x^{\text{PK}} = 2\mu b\varepsilon_{xy}^{bg}$ is the PK force, as obtained from Eq. (4) for this case, and the other terms of the right-hand side represent the core force $f_x^{\text{core}}$ of Eq. (3). In Eq. (9), the strains and their derivatives are evaluated at the dislocation position.

### B. Numerical precision in the measurings of the core-force properties

Quantitative investigations about the influence of the background strain derivatives on dislocation dynamics are not straightforward to do. They obviously require the precise knowledge of the background strain fields on each dislocation and of the core force acting on it.

In this section, we explain how to obtain, in simulations, precise measures of the dislocation position, the background strains on it, and the resulting core force.

#### *1. Dislocation position*

In order to study the glide movement, we need a correct way to identify the position of a dislocation along its glide line. By showing Voronoi diagrams of crystal configurations, Fig. 2 illustrates how such movement occurs.

In Fig. 2(a), a PK force to the left is counterbalanced by a core force to the right. Then, by slightly increasing the background strain gradient at the dislocation position, we increase a little the core force. As a consequence, the dislocation "moves" to the right until it reaches a position where the forces equilibrate again. The resulting configuration is shown in Fig. 2(b). The "movement" turns out to be a tilting of the line connecting the disclination particles, which are the particles that represent the dislocation in a Voronoi tesselation and have 5 (red) and 7 (blue) neighbors. On the right side of Fig. 2, the line connecting disclination particles is compared with a vertical dotted line in order to show the tilting. By comparing Figs. 2(a) and 2(b), we can hardly say how much the dislocation "moved" in the glide direction (i.e., in the $x$ direction). The unique visible difference is that the disclination particles are vertically aligned in Fig. 2(a) and tilted to the right in Fig. 2(b). By repeating the procedure, increasing the core force and waiting equilibration, we obtain the configuration in Fig. 2(c). In this case, there occurred a change in the disclination particles but they continue to be tilted (this time to the left). Repeating of the procedure again now tilts the disclinations to the right, as shown in Fig. 2(d).

From Figs. 2(a) to 2(d), the dislocation moved. If we define the dislocation position as simply the mean position between the disclination particles, the dislocation movement would be discontinuous, having a hop from Fig. 2(b) to 2(c). But the system configuration changes continuously. There may be a way to define the dislocation position such that it changes continuously during the glide. This would be a more appropriate definition to be used when comparing simulation results with a theory (which is continuous). Without knowing such definition, only in cases as the one in Fig. 2(a) we can precisely locate the dislocation position along the $x$ direction, due to the vertical alignment of the disclinations.

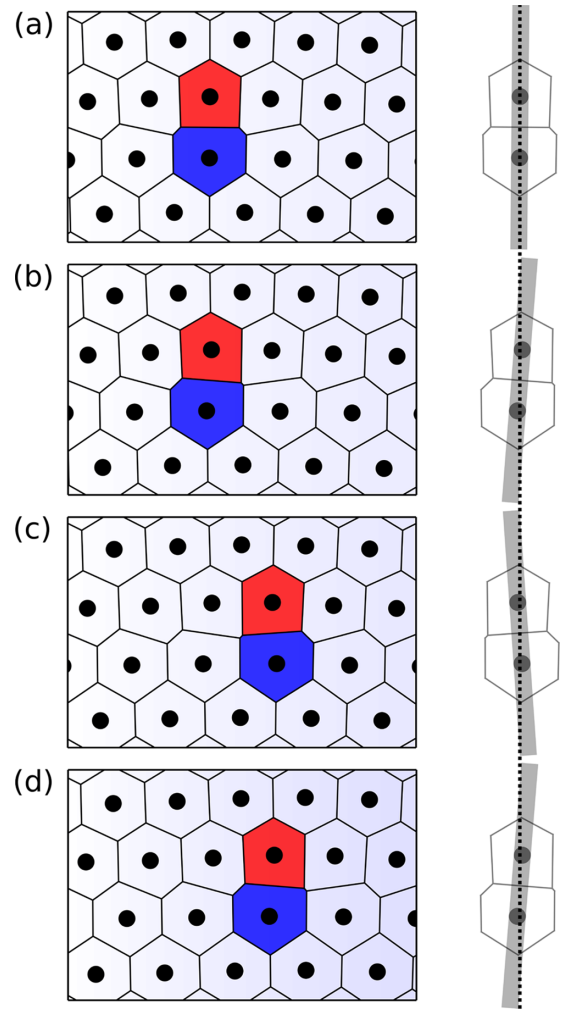


FIG. 2. Steps of an adiabatic dislocation glide in the $x$ direction, as observed in a simulation. The Voronoi diagrams have the same coloration as in Fig. 1. In (a), a PK force to the left is counterbalanced by a core force to the right. In the subsequent steps, we increase the core force by slightly increasing the background strain gradient at the dislocation position and wait till the configuration equilibrates. The resulting configuration of each step is shown in (b), (c), and (d). The dotted vertical line on the right is a guide to the eye in order to show the "tilting" of the dislocation at each step of the glide.

In our simulations, we choose to consider only the situations in which the disclinations are aligned perpendicularly to the glide line. Therefore, in the glide of Fig. 2, we would consider the configuration 2(a) and a configuration that is between Figs. 2(c) and 2(d) and for which the vertical alignment happens. The disclinations' positions then provide the exact dislocation position along the glide line. When they are not aligned in this way, we have some uncertainty about the dislocation position. Our investigations need an uncertainty much smaller than the lattice constant.

#### 2. Background strains

A direct observation of the crystal configuration around a dislocation provides the *total* strain fields. These are the resulting deformations generated by all the sources of strains, such as the dislocation itself, other defects, boundary conditions, external body force fields, etc.

In order to evaluate only the background strain fields on a given dislocation (i.e., the ones generated by all the sources except by the dislocation itself), we need to use a theoretical framework that gives how each source (or group of sources) of strain acts. This can easily be done if the system is well described by the classical linear hyperelasticity (or simply classical elasticity) theory of elastic deformations. This is the case for our simulations, which occurs in the linear regime.

#### 3. Core-force magnitude

In general, the PK and the core forces act simultaneously to drive the dislocation. Classical elasticity can be used to evaluate the PK force with good approximation. Resistances to movements may also be present. By knowing the PK and the resistances and by measuring the total force, we can obtain the core force.

But, without knowing the correct mobility law of dislocation dynamics in the system, we cannot measure the total force on the dislocation by measuring its movement, unless the system is in static equilibrium, and then the total force is certainly zero. This also avoids the consideration of nonequilibrium effects in the theory. Also, if the resistances to movement are negligible, equations simplify even more and, in equilibrium, we have that the core force is simply the negative of the PK force.

Our simulations use equilibrium situations of a system with negligible resistances to movement. In these cases, we use classical elasticity to evaluate the PK force and then obtain the core force, which is simply the negative of $\mathbf{f}^{\mathrm{PK}}$.

### C. Simulation setup

In our simulations, we use a model system in which we can probe all the properties of the core force (listed in Sec. II) and also measure its magnitude. It takes the precautions commented in the previous subsection for having better precisions in the numerical results. It also enables us good control over the system, allowing us to probe the core-force properties. In the following, we describe our system and its advantages in having good knowledge and control over the strain fields and the dislocation positions.

In Sec. III C 1, we tell the pair interaction between the particles and explain how its choice facilitates us to probe properties (i), (ii), (iii), and (v) of Sec. II. Then Secs. III C 2 and III C 3 describe the boundary conditions and the dislocations' configuration, and how they facilitate the measure of the core-force magnitude and the check of properties (ii), (iv), and (v). These properties are also more easy to check with the the external body force described in Sec. III C 4.

#### 1. Interparticles' interactions

The simulations have particles with power-law repulsive interactions $V_p(r) = U_0(a_0/r)^{12}$. Interactions like this have been used as a simple model in many situations, including dislocation studies [47,48]. In Sec. I of the Supplemental Material (SM) [49], we derive analytical expressions for the bulk and shear moduli [50] resulted from this interaction.

Such type of system is useful for our analysis due to its easiness for dislocation glide (i.e., a low Peierls-Nabarro barrier, as observed in our results), facilitating the check of the effective action of a driving force such as the core force, i.e., property (i) of Sec. II. In this case, the action can happen for small strain gradients, avoiding nonlinear effects and allowing us to test the linearity (ii) property.

Moreover, the negligible Peierls-Nabarro barrier avoids the hysteresis in the movement which can appear due to the barrier. Consequently, an adiabatic "come and go" movement of the dislocation will not have hysteresis unless the force on it is not uniquely determined by the current configuration. This checks the uniqueness (iii) property.

Finally, the short-ranged character of the interaction facilitates us to probe the locality (v) property. Otherwise, in a possible occurrence of nonlocal effects, we could not track at first if their origin is in the core force or in the interparticles' interaction.

#### 2. Periodic boundary conditions

Since the particles in our simulations are repulsive, they must be confined physically or by the use of periodic boundary conditions (PBC). In a physical confinement, the theory could not considerate the discretization effects in the boundary precisely since the edge has irregularities due to the crystal structure.

Therefore, we use PBC in which the theory is more precise, helping us to probe the linearity (ii) and locality (v) properties commented in Sec. II. We simulate $N = 49\,152$ particles in a rectangular cell $(x, y) \in [-L_x/2, L_x/2] \times [-L_y/2, L_y/2]$ with $L_x = 192a_0$ and $L_y = 256(\sqrt{3}a_0/2)$, where $a_0$ is the lattice spacing.

#### 3. Dislocation dipole

The PBC constrain the total Burgers vector to be zero. Therefore, other types of source for background strains must appear: Other defects. We consider simulations in which we take a perfect crystal and nucleate a dipole of dislocations. They are formed in the slip line $y = 0$, have Burgers vectors $\mathbf{b} = \pm a_0\hat{\mathbf{x}}$ and positions $x = \pm d/2$, respectively, where $d$ is the distance between them.

Figure 3 illustrates the configuration of the dislocations and their images due to the PBC. The symmetric configuration in our system helps us to probe the property (iv) commented in Sec. II, i.e., the symmetry of the core force under Burgers vector inversion.

The background shear strain $\varepsilon_{xy}^{bg}$ at each dislocation induced by the dipole formation and the PBC is derived in the SM [49] and is given by

$$\varepsilon_{xy}^{bg} = -\frac{a_0 d}{2L_x L_y} - \frac{\pi\beta a_0}{2L_y^2}\sum_{n\in\mathbb{Z}}(d + nL_x)\mathrm{csch}^2\left[\pi\frac{(d + nL_x)}{L_y}\right], \tag{10}$$

where $\beta = B/(B + \mu)$. The first term on the right-hand side of Eq. (10) is a result of the negative resolved shear induced

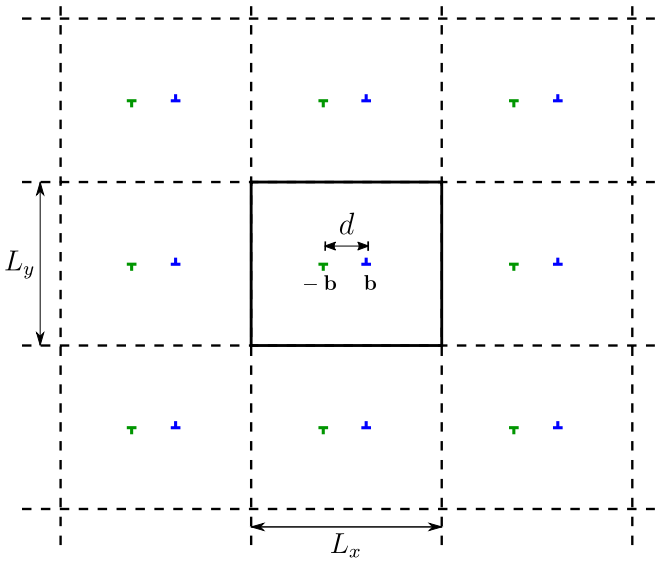


FIG. 3. Simulation box (the central one in the figure) and its images due to the PBC. In a horizontal slip line, a dipole of dislocation is formed within the perfect crystal. Then we use PK and core forces to control the dislocations' positions.

by the gliding of the dislocations from the nucleation point until their current positions (separated by $d$), in the sense of what is shown on the right side of Fig. 1. Details are given in the SM [49], where we use closed-form expressions for some infinite series as it has been used in the context of dislocation dipoles in PBC [51,52].

#### *4. External-body force field*

Each dislocation of the dipole in PBC is subjected to a PK force of attraction to the other one. They tend to annihilate each other and return the crystal to its perfect configuration. External-body force fields can be used in order to induce background strain fields that act as configurational forces and counteract the attraction between the dislocations, keeping them apart from each other at a fixed distance $d$. The configurational force that we intend to induce is the core force.

We induce appropriate strain gradients in the system using one-dimensional (1D) and radial external-body forces. We use $V_{\rm ext}^{\rm 1D}(x) = V_0 v(x/l)$ and $V_{\rm ext}^{\rm rad}(r) = V_0 v(r/l)$, where $v(x) = x^8(\kappa e^{-\kappa x^{10}} - e^{-x^{10}})$, $\kappa = 0.35$ and $r = \sqrt{x^2+y^2}$. We simulate for different values of the length parameter $l$, namely, $l = 55a_0$, $57a_0$, and $59a_0$.

We observed that, for these choices of external potential, the dislocations can be kept apart with sufficiently small strains and strain derivatives in the system, allowing the usage of classical elasticity with good approximation. Such regime allows us to probe the linearity (ii) property of the core force, as commented in Sec. II. The induced background strains also have enough variation within a few lattice spacings, allowing us to probe the locality (v) property. We can use Eq. (8) to evaluate such strains. They are given by

$$\varepsilon_{xx}^{bg}(x) = \frac{\rho_0 V_{\rm ext}^{\rm 1D}(x)}{B+\mu} \tag{11}$$

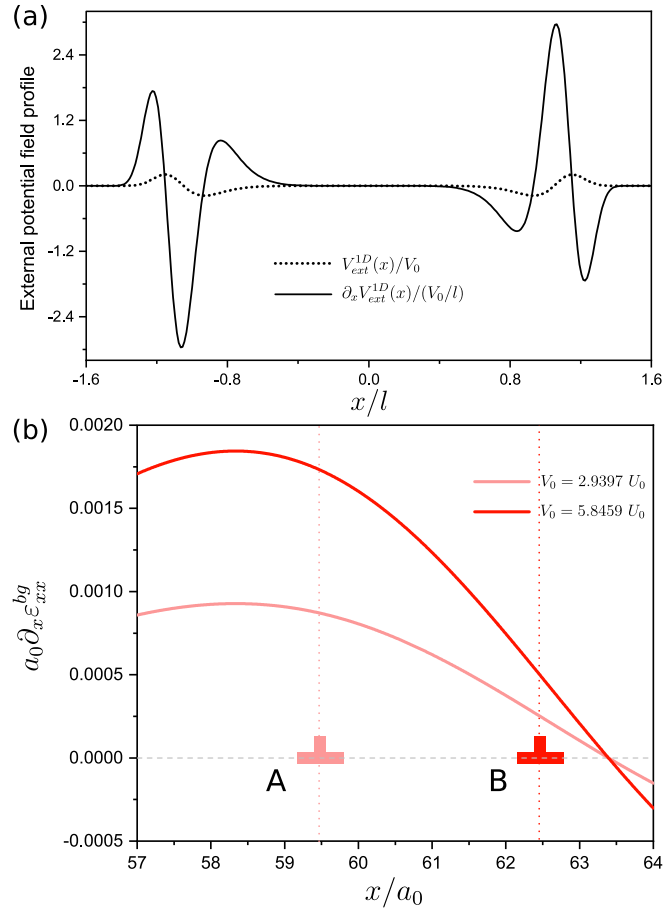


FIG. 4. (a) Profile of the external potential field $V_{\rm ext}^{\rm 1D}(x) = V_0 v(x/l)$, where $v(x) = x^8(\kappa e^{-\kappa x^{10}} - e^{-x^{10}})$ and $\kappa = 0.35$, and of its derivative, used in our simulations. (b) Plot of $a_0\partial_x\varepsilon_{xx}^{bg}(x)$ for the system under action of $V_{\rm ext}^{\rm 1D}(x)$, as derived from Eq. (11), with $l = 55a_0$, $V_0 \approx 2.94U_0$ (light red), and $V_0 \approx 5.85U_0$ (dark red). For these values of $V_0$, we observe the dislocations to equilibrate, respectively, at $x \approx \pm 59.5a_0$ and $x \approx \pm 62.5a_0$, as shown by A and B. The plot is shown near the position of the dislocation on the right side.

and $\varepsilon_{yy}^{bg} = \varepsilon_{xy}^{bg} = 0$ in the 1D case and by

$$\varepsilon_{yy}^{bg}(x) = \frac{\rho_0}{(B+\mu)}\frac{1}{x^2}\int_0^x x' V_{\rm ext}^{\rm rad}(x')dx', \tag{12}$$

$$\varepsilon_{xx}^{bg}(x) = \frac{\rho_0 V_{\rm ext}^{\rm rad}(x)}{B+\mu} - \varepsilon_{yy}^{bg}(x), \tag{13}$$

and $\varepsilon_{xy}^{bg} = 0$ in the radial case.

Figure 4(a) shows the profile of $V_{\rm ext}^{\rm 1D}$ and its derivative. The symmetry of the external potential is convenient in order to test the core-force symmetry under Burgers vector inversion [property (iv) commented in Sec. II]. It is also convenient in the identification of dislocation positions since the alignment commented in Sec. III B 1 occurs simultaneously for both the dislocations.

## IV. SIMULATION RESULTS

As previously commented, we consider only the situations in which the dislocations are at rest. Then, by analyzing

different situations like this, we can obtain how the different contributions to the force counterbalance each other. By changing the strain gradients (e.g., through a change in $V_0$) that are responsible for the core-force contribution, the dislocations are driven to the new positions where the resulting force is zero and they equilibrate. In fact, by increasing the core force, the dislocations are driven apart, i.e., in a direction that is opposite to the PK force. This observation confirms the property (i) of Sec. II, i.e., that the core force is not a drag force but a driving one.

In our simulations, the resulting force on the dislocations is always able to drive them back and forth without any sign of hysteresis, indicating that the Peierls-Nabarro barrier is very small. This also confirms the property (iii) of Sec. II, i.e., the uniqueness of the core force. From one equilibrium configuration to the other we use overdamped evolution for the particles in the simulations. No unstable equilibrium appears, as we probed by using a small temperature through Brownian dynamics [53].

For the system in which we apply $V_{\rm ext}^{\rm 1D}(x)$ with $l = 55a_0$, Fig. 4(b) shows the graph of the strain gradient $a_0\partial_x\varepsilon_{xx}^{bg}$, as generated by the external force and evaluated through Eq. (11), near the position at which the dislocation $\mathbf{b} = +a_0\hat{\mathbf{x}}$ is equilibrated in our simulations with $V_0 \approx 2.94U_0$ (light red) and $V_0 \approx 5.85U_0$ (dark red). In this region, $\varepsilon_{xy}^{bg} < 0$ and then, if we turn off the external force (i.e., set $V_0 = 0$), the dislocation shown in the figure would move to the left until it finally annihilates the other dislocation, which would be precisely at $x = 0$. We can see in the figure that, by increasing $V_0$, the strain gradient increases and the dislocation moves to the right until it equilibrates in a new position. The same happens simultaneously with the other dislocation in the other direction. This mirror symmetry, observed in all simulations, confirms the property (iv) of Sec. II, i.e., the Burgers vector inversion symmetry of the core force.

We gather the data of equilibrium situations (i.e., dislocations at rest with $f_x^{\rm disl} = 0$) in varying intensities of $V_{\rm ext}^{\rm 1D}(x)$ for the three different values of the parameter $l$ considered. As we consider only the cases in which the dislocation positions are well defined, as commented in Sec. III B 1, their distances can be precisely evaluated. For these cases, we use Eqs. (10) and (11) to evaluate the background deformations and plot in Fig. 5(a) the values of $-2\varepsilon_{xy}^{bg}$ versus $a_0\partial_x\varepsilon_{xx}^{bg}$ acting at the dislocations' equilibrated positions. Note that a linear relation is predicted for this graph if we consider Eq. (9) up to first gradient. A simple fit results in $M_{xx} \approx 1.64\mu a_0^2$, but we clearly see that the force counteracting the PK one does not depend solely on the value of $\partial_x\varepsilon_{xx}^{bg}$.

In principle, the problem here could have a nonlocal origin, as we can see from Fig. 4(b) that the strain derivative varies greatly within a few lattice spacings. But we find that, by considering higher-order derivative terms in Eq. (9) evaluated precisely at the dislocation positions, we can match the data with a good fit and then the locality property (v) of Sec. II is valid. The motivation to consider the higher-order derivative terms is discussed in the following.

The cases A and B of Fig. 5(a) are the same of Fig. 4(b). In the transition from A to B, the dislocations are driven apart and their new equilibrium positions have smaller $|\partial_x\varepsilon_{xx}^{bg}|$. If

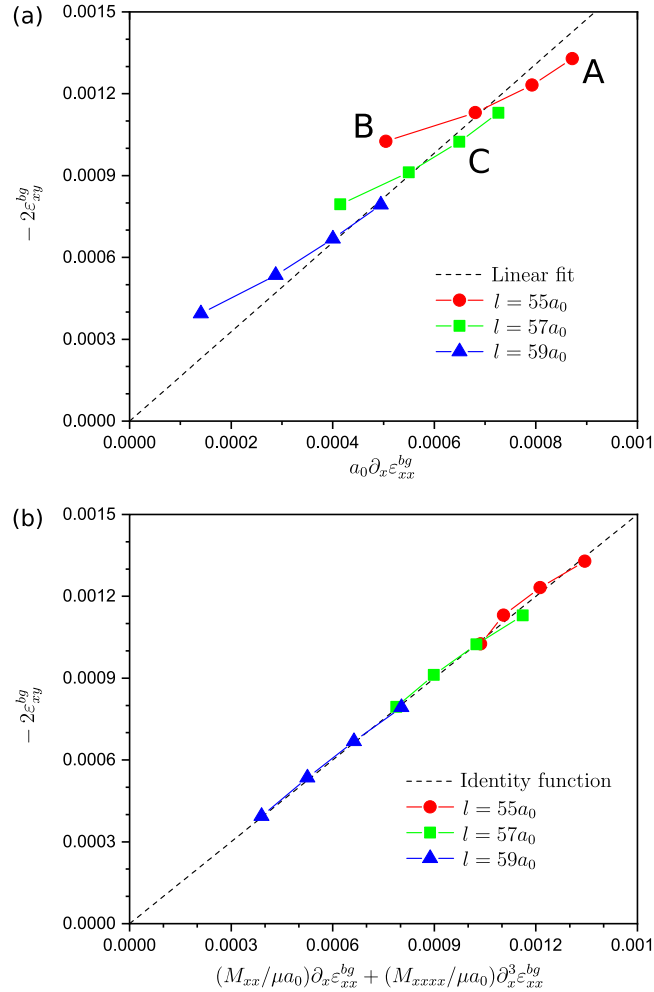


FIG. 5. Relations between the background-resolved shear and strain gradients on the dislocation $\mathbf{b} = +a_0\hat{\mathbf{x}}$ for equilibrium configurations in our simulations with the 1D external force field. All the deformations can be obtained from the distance between the dislocations using Eqs. (10) and (11). In (a) we can see that $\partial_x\varepsilon_{xx}^{bg}$ alone cannot explain the force which is counterbalancing the PK one. By including a force due to $\partial_x^3\varepsilon_{xx}^{bg}$, a good fit to the data is obtained, as it is shown in (b).

we compare the cases B and C, where C was simulated with a different external force field, we can see that the PK forces (originated from $\varepsilon_{xy}^{bg}$) in them are almost equal, whereas the strain gradients $\partial_x\varepsilon_{xx}^{bg}$ are different. Thus, the core force that counterbalances PK must depend on other factors that are different in these cases, such as the higher-order derivatives $\partial_x^2\varepsilon_{xx}^{bg}$ and $\partial_x^3\varepsilon_{xx}^{bg}$. Locally, these derivatives are the main differences between the situations B and C of Fig. 4(a) aside from the difference in $\partial_x\varepsilon_{xx}^{bg}$. We can better fit the data by considering, for instance, an additional contribution like $M_{xxx}\partial_x^2\varepsilon_{xx}^{bg}$ (provided that $M_{xxx}$ changes sign under a change in the sign of $b$) or $M_{xxxx}\partial_x^3\varepsilon_{xx}^{bg}$ in the force of Eq. (9).

In the end of Sec. V B 1, we show some theoretical arguments that make us believe that the core force cannot be linear with $\partial_x^2\varepsilon_{xx}^{bg}$ and thus $M_{xxx}$ must be zero. Using only the $M_{xx}$ and $M_{xxxx}$ terms in Eq. (9), the fitting of the data provides

$M_{xx} \approx 2.259\mu a_0^2$ and $M_{xxxx} \approx 7.023\mu a_0^4$. Figure 5(b) shows how the formula for the force is greatly improved by the third gradient term. Note that all the terms used here are linear in the strains, confirming the property (ii) of Sec. II, i.e., the linearity of the core force.

Finally, we use the data for the simulations with radial forces (in which there appears $\varepsilon_{yy}^{bg}$) and fit the general equilibrium condition

$$f_x^{\text{disl}} \approx 2\mu b\varepsilon_{xy}^{bg} + M_{xx}\partial_x\varepsilon_{xx}^{bg} + M_{yy}\partial_x\varepsilon_{yy}^{bg} + M_{xxxx}\partial_x^3\varepsilon_{xx}^{bg} + M_{xxyy}\partial_x^3\varepsilon_{yy}^{bg} = 0 \tag{14}$$

to obtain the values $M_{yy} \approx 0.5024\mu a_0^2$ and $M_{xxyy} \approx -17.57\mu a_0^4$. The other background strain derivatives were not considered since their values are relatively much smaller in our system.

## V. THEORETICAL APPROACHES

In this section, we investigate some theoretical predictions about the core force that are found in the literature and also other possibilities. Unfortunately, all of them have issues and none of them were found to predict the coefficients of the core force without a direct measurement from the simulations. But many properties are correctly predicted and some interesting results are found.

We can separate the theoretical approaches into two types: Continuum theory modifications and core-energy analysis. Any type of continuum theory of elasticity is an approximation and its prediction about the dislocation energy must be complemented by a core-energy correction. In Sec. V A, we show some efforts to modify the classical elasticity theory in order to better describe the dislocation dynamics, without resorting to core-energy considerations. In Sec. V B, we focus on the core-energy consideration and try to find ways of measuring it in order to predict the core force. Also, we show a case in which we can go the other way around, i.e., use the coefficients in the core force to evaluate the core energy.

### A. Modifications within continuum theory

The dislocation energy within the continuum elasticity theory depends on the energy functional and on how the dislocation is described. In order to obtain the core force, here we investigate possible modifications of the functional or of the dislocation description.

#### *1. Energy functional modifications*

The Peach-Koehler force results from the classical elasticity functional, expressed in Eq. (7), and the Burgers vector definition $\mathbf{b} = \oint d\mathbf{u}$. In the SM [49], we derive it together with a possible modification in the energy functional which can provide strain gradient forces without using a core-energy correction but adding a term like $-C_{ijklm}^{(1)}\varepsilon_{ij}\partial_m\varepsilon_{kl}/2$, where $C_{ijklm}^{(1)}$ are constants, inside the integral (7). This modification is a type of strain gradient theory (SGT), that is, a continuum theory that considers relevant influences of strain gradients in the elasticity and plasticity. The correction to the PK force derived in the SM [49] is

$$f_n^{\text{SGT}} = \epsilon_{nk}b_l C_{ijklm}^{(1)}\partial_m\varepsilon_{ij}^{bg}, \tag{15}$$

where $\boldsymbol{\epsilon} = \left[\begin{smallmatrix} 0 & 1 \\ -1 & 0 \end{smallmatrix}\right]$. It obeys properties such as uniqueness, locality, and linearity but it has problems with the symmetry under the inversion $\mathbf{b} \to -\mathbf{b}$ [property (iv) of Sec. II], which was confirmed by our simulations to be valid in the core force.

SGTs of elasticity which correctly obey the symmetries have long been studied [54,55]. For example, we can add a term $\propto \partial_k\varepsilon_{ij}\partial_n\varepsilon_{lm}$ in (7), which correctly obeys the symmetries, and obtain $\mathbf{f}^{\text{disl}}$ through a procedure similar to the one used in the SM [49]. The resulting force has a term proportional to second gradients of strains. This second gradient force is similar to the third term in the right-hand side of Eq. (9) and is originated from a generalized elasticity theory, without considering the core energy. Unfortunately, no correct account for a first gradient force on dislocations, with the properties that we observe in this work, was ever obtained in this way.

Another possible correction within continuum theory is to consider nonlinear terms in the energy functional. But, the formal derivations of the configurational force in nonlinear elasticity [56] provide only nonlinear corrections to PK, which disobey the property (ii) of Sec. II, and have no strain gradient dependence.

#### *2. A modification in the dislocation description: The core field*

We can try to correct the classical elasticity by modifying the way we characterize a dislocation. To do so, we present here an approach that provides a prediction of the core force, as derived in [34]. But, as commented further in the end of this subsection, we observe that it cannot predict the correct coefficients of the core force, and therefore it is quantitatively wrong.

The classical (Volterra) displacement field $\mathbf{u}^V$ of a dislocation at the origin is the solution of the equations

$$\epsilon_{jk}\partial_j\partial_k u_i^V = b_i\delta(\mathbf{r}) \quad \text{and} \quad C_{ijkl}\partial_j\partial_l u_k^V = 0. \tag{16}$$

The first equation comes from the Burgers vector definition and the second one is the classical elasticity field equation (8) for zero body forces. In polar coordinates, the Volterra field has the form

$$\mathbf{u}^V(r,\theta) = \mathbf{v}(\theta)\ln r + \mathbf{u}_0(\theta). \tag{17}$$

A simple way to modify such dislocation description is to consider that there are some forces acting near the dislocation core. Thus, the so-called core field $\mathbf{u}^{cf}$, which is the solution of

$$C_{ijkl}\partial_j\partial_l u_k^{cf} = -f_i^{cf}, \tag{18}$$

must be considered in order to correct the Volterra approximation. Here, $\mathbf{f}^{cf}(\mathbf{r})$ is an *ad hoc* body force density field associated with the dislocation. In the literature [34,41], $\mathbf{f}^{cf}(\mathbf{r})$ is usually considered as a set of point forces. This force field does not necessarily have a physical existence. It is used here as a mathematical tool to obtain the core field, which has physical existence. Consequently, this force field accompanies the dislocation during the motion, being a function of $\mathbf{r} - \mathbf{r}^d$.

Note that the net contribution of $\mathbf{f}^{cf}$ must be zero, i.e., $\int \mathbf{f}^{cf}(\mathbf{r})d^2r = 0$, since no net force appears in the dislocation region. Moreover, as it represents a core effect, this force must be zero outside some core radius, where classical elasticity is valid. Therefore, the core field decays rapidly and has the following multipole expansion:

$$\mathbf{u}^{cf}(r,\theta) = \mathbf{u}_1(\theta)\frac{1}{r} + \mathbf{u}_2(\theta)\frac{1}{r^2} + O\left(\frac{1}{r^3}\right), \tag{19}$$

where $\mathbf{u}_1$ and $\mathbf{u}_2$ depend on the dipolar and quadrupolar moments of $\mathbf{f}^{cf}(\mathbf{r})$, respectively.

Other constraints on $\mathbf{f}^{cf}$ are necessary in order to obey the reflection symmetry of the edge dislocation. For the case $\mathbf{b} = b\hat{\mathbf{x}}$, we must have $\mathbf{f}^{cf}(\mathbf{r}) = \boldsymbol{P}\cdot\mathbf{f}^{cf}(\boldsymbol{P}\cdot\mathbf{r})$ for the reflection (parity) operation $\boldsymbol{P} = \left[\begin{smallmatrix}-1 & 0\\ 0 & 1\end{smallmatrix}\right]$, i.e., $f_x^{cf}(x,y) = -f_x^{cf}(-x,y)$ and $f_y^{cf}(x,y) = f_y^{cf}(-x,y)$. In this case, the contribution to the energy due to $\mathbf{f}^{cf}$ interacting with the background deformation can be directly obtained from the energy functional (7). We can make a multipole expansion and use the symmetries to simplify it, obtaining

$$\begin{aligned} E^{cf\text{-}bg} &= -\int f_i^{cf}(\mathbf{r})u_i^{bg}(\mathbf{r})d^2r \\ &\approx -\big[M_1\partial_x u_x^{bg} + M_2\partial_y u_y^{bg} + M_{12}\partial_x\partial_y u_x^{bg} + M_{11}\partial_x^2 u_y^{bg} \\ &\quad + M_{22}\partial_y^2 u_y^{bg} + M_{111}\partial_x^3 u_x^{bg} + M_{112}\partial_x^2\partial_y u_y^{bg} \\ &\quad + M_{122}\partial_x\partial_y^2 u_x^{bg} + M_{222}\partial_y^3 u_y^{bg} + O(\partial^4 u^{bg})\big], \end{aligned} \tag{20}$$

where $M_1 = \int x f_x^{cf} d^2r$, $M_2 = \int y f_y^{cf} d^2r$, $M_{12} = \int xy f_x^{cf} d^2r$, $M_{11} = \int (x^2/2) f_y^{cf} d^2r$, $M_{22} = \int (y^2/2) f_y^{cf} d^2r$, $M_{111} = \int (x^3/6) f_x^{cf} d^2r$, $M_{112} = \int (x^2 y/2) f_y^{cf} d^2r$, $M_{122} = \int (xy^2/2) f_x^{cf} d^2r$, and $M_{222} = \int (y^3/6) f_y^{cf} d^2r$. Also, by symmetry, a change in the sign of $b$ changes the sign of the quadrupolar moments $M_{12}$, $M_{11}$, and $M_{22}$ in Eq. (20).

The derivatives in Eq. (20) are evaluated at the dislocation position and then the energy varies as the defect moves. From Eq. (1), such variation of $E^{cf\text{-}bg}$ implies in a force acting on the dislocation which has the same form of Eq. (3) and satisfies all the properties guessed in Sec. II and confirmed in Sec. IV. Up to first gradients of strains, this approach gives

$$f_x^{\text{disl}} \approx 2\mu b\varepsilon_{xy}^{bg} + M_1\partial_x\varepsilon_{xx}^{bg} + M_2\partial_x\varepsilon_{yy}^{bg}. \tag{21}$$

This approach predicts that the coefficients appearing in the core force are the moments of $\mathbf{f}^{cf}(\mathbf{r})$ that appear in the core field. In principle, these moments can be measured by comparing the theoretical dislocation field $\mathbf{u}^d = \mathbf{u}^V + \mathbf{u}^{cf}$ with the one observed in the crystal, as long as the core-field consideration is a good way to correct the Volterra approximation. In the SM [49], we analyze this through simulation. Unfortunately, we observed that the correct coefficients for the core force measured through simulations (Sec. IV), i.e., $M_{xx}$ and $M_{yy}$, cannot be obtained by the core-field analysis.

### B. Core energy as the origin of the core force

This section investigates the core energy and its relation with the core force. Note that all the properties of the core force guessed in Sec. II (i.e., effective driving action, linearity, uniqueness, etc.) and confirmed in Sec III are obeyed if we write the force (3) in the form

$$\mathbf{f}^{\text{core}} = -\frac{\partial E^{\text{co}}}{\partial \varepsilon_{ij}^{bg}}\nabla\varepsilon_{ij}^{bg} - \frac{\partial E^{\text{co}}}{\partial\left(\partial_k\varepsilon_{ij}^{bg}\right)}\nabla\partial_k\varepsilon_{ij}^{bg} - \cdots, \tag{22}$$

where we only need to know how to evaluate the crystal's core-energy function $E^{\text{co}} = E^{\text{co}}(\varepsilon_{ij}^{bg}, \partial_k\varepsilon_{ij}^{bg}, \dots)$ in a unique way.

In the following, Sec. V B 1, a general definition of the core energy is given. The final evaluation of it depends on how the continuum theory is considered. Section V B 2 shows the standard way to do so and its problems with ambiguity are commented. Finally, in Sec. V B 3, we show that, in systems with power-law interactions, we can obtain the core energy from measurements of the core force.

#### 1. General definition of the core energy

The general idea for the core energy ($E^{\text{co}}$) is that it represents the energetic correction necessary for the continuum theory result ($E^{\text{cont}}$) to match the total dislocation energy ($E^{\text{disl}}$) in the real crystal, i.e., $E^{\text{disl}} = E^{\text{cont}} + E^{\text{co}}$.

The crystal's $E^{\text{disl}}$ has a definite way to be evaluated. It is obtained from the total energy of the crystal when deformed by the dislocation presence minus the energy of the crystal without it. By considering the crystal's energy as a function of the particles' positions, we can write

$$E^{\text{disl}} = E(\{\mathbf{r}^\alpha\}) - E(\{\mathbf{r}^{\alpha,0}\}), \tag{23}$$

where $\{\mathbf{r}^\alpha\}$ and $\{\mathbf{r}^{\alpha,0}\}$ are the particles' positions with and without the dislocation presence, respectively. The evaluation of $E^{\text{cont}}$, on the other hand, depends on the theory considered and the standard one is presented in Sec. V B 2.

In practice, $E^{\text{disl}}$ increases with the size of the crystal, diverging for infinite crystals. The continuum theory prediction also diverges while the core energy is finite. Therefore, we consider energetic evaluations inside a circular region, with radius $R$ and centered at the dislocation, and define

$$E^{\text{co}} = \lim_{R\to\infty}[E^{\text{disl}}(R) - E^{\text{cont}}(R)]. \tag{24}$$

The convergence of this limit is usually fast, as the continuum theory rapidly becomes accurate far from the core.

The presence of background strains can affect the core energy and some symmetric considerations can be made *a priori*. For an edge dislocation with $\mathbf{b} = b\hat{\mathbf{x}}$, e.g., linear dependencies of $E^{\text{co}}$ on $\varepsilon_{xy}^{bg}$ and $\partial_x\varepsilon_{xx}^{bg}$ are forbidden, as we can see from Fig. 6. Consequently, the force obtained from Eq. (22) does not have terms linearly proportional to $\partial_x\varepsilon_{xy}^{bg}$ or to $\partial_x^2\varepsilon_{xx}^{bg}$. Note that Eq. (20) does not represent the core energy since it is zero when there is no background deformation, but it carries all the symmetries expected for $E^{\text{co}}$.

#### 2. Ambiguity in the standard core energy

The standard way to evaluate the continuum theory prediction $E^{\text{cont}}$ for the dislocation energy is through Eq. (7), by using the dislocation strains in the integral. The classical strain fields of a dislocation are obtained from the Volterra solution of Eq. (16). In polar coordinates, there exist functions $h_{ij}^V(\theta)$ such that the solution for a dislocation $\mathbf{b} = b\hat{\mathbf{x}}$ at the origin has

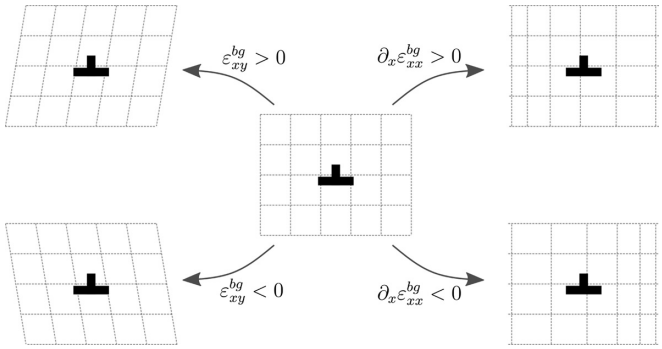


FIG. 6. Illustration of the effects of $\varepsilon^{bg}_{xy}$ and $\partial_x \varepsilon^{bg}_{xx}$ around an edge dislocation. The reflection symmetry in the $x$ direction implies that the change in the core energy must be the same for positive and negative values of these deformations. Therefore, this energy cannot depend linearly on them.

the form [4]

$$\varepsilon^V_{ij}(\mathbf{r}) = h^V_{ij}(\theta)\frac{b}{r}. \tag{25}$$

Note that the integral of Eq. (7) using Volterra strains diverges logarithmically for both large and small radii. The usual procedure to obtain $E^{\rm cont}$ is to integrate Eq. (7) in a region between a fixed core radius $r^{\rm co}$ and a larger radius $R \gg r^{\rm co}$. By doing so, the core energy is standardly defined as [4]

$$E^{\rm co,std} = \lim_{R\to\infty}\left[E^{\rm disl}(R) - \frac{b^2 K}{8\pi}\ln\left(\frac{R}{r^{\rm co}}\right)\right], \tag{26}$$

where the prelogarithmic factor $K$ depends on the elastic constants, e.g., $K = 4B\mu/(B+\mu)$ for the triangular crystal.

The choice of the core radius $r^{\rm co}$ is arbitrary and usually taken to be of the order of the Burgers vector modulus $b$, which is frequently the lattice spacing. By taking simulations for large values of $R$ and using the correct $K$, Eq. (26) converges and $E^{\rm co,std}$ is then independent of $R$ [57]. See [35,39,58] for some recent calculations of $E^{\rm co,std}$ from simulations of straight dislocations in some relevant 3D crystals.

In order to obtain the core force through Eq. (22), we need to know how the core energy depends on the background strains. By using background deformations in the defected crystal of the simulation and measuring the corresponding core energies, the dependence $E^{\rm co,std} = E^{\rm co,std}(\varepsilon^{bg}_{ij})$ can be evaluated, as it was done in previous works [35,38]. These works used the evaluated derivatives of $E^{\rm co,std}(\varepsilon^{bg}_{ij})$ to predict the core force, through Eq. (22). But this core-energy definition has problems with uniqueness, i.e., with the property (ii) of Sec. II, as we discuss in the following.

The standard core energy greatly depends on the choice of the core radius. Once measured for some $r^{\rm co}$, the energy $\overline{E}^{\rm co,std}$ for any other core radius is $\overline{E}^{\rm co,std} = E^{\rm co,std} + (b^2K/8\pi)\ln(\bar{r}^{\rm co}/r^{\rm co})$. Since the factor $b^2K$ is also a function of the background strains, in general, we have that $\partial\overline{E}^{\rm co,std}/\partial\varepsilon^{bg}_{ij} \neq \partial E^{\rm co,std}/\partial\varepsilon^{bg}_{ij}$. This means that the arbitrary choice of $r^{\rm co}$ affects the dependence $E^{\rm co,std} = E^{\rm co,std}(\varepsilon^{bg}_{ij})$ and the core force of Eq. (22). As uniqueness is a confirmed property of the core force, the standard core energy is not appropriate, due to its ambiguous definition, to be used in Eq. (22).

There are some known definitions for the core energy which are unambiguous, e.g., in the framework of the KTHNY theory [36] and in the Kanzaki force approach [37]. The correct one to be used in Eq. (22) and then predict the correct core force acting on a dislocation is still to be discovered.

### 3. *Crystals with power-law interactions: Obtaining the core energy from the core force*

By considering that Eq. (22) is valid, the measured coefficients of the core force give us the derivatives of $E^{\rm co,std} = E^{\rm co,std}(\varepsilon^{bg}_{ij}, \partial_k\varepsilon^{bg}_{ij}, \dots)$. Here we show that there are systems in which we can obtain the absolute value of the core energy directly from its derivatives. In such cases, the core energy can be obtained from measures of the core force. This happens in systems with power-law interactions, which are known to have special relations, such as the virial theorem, between energy and force.

If the particles interact via a power-law potential $V_p(r) \propto 1/r^m$, we have the scaling law $E(\{\lambda\mathbf{r}^\alpha\}) = \lambda^{-m}E(\{\mathbf{r}^\alpha\})$ for the total potential energy. This is satisfied by $E^{\rm disl}$, as we can see from Eq. (23), by $E^{\rm cont}$, which comes from a continuum theory, and therefore by $E^{\rm co} = E^{\rm disl} - E^{\rm cont}$. The scaling law describes how these energies depend on the density, which scales as $\lambda^{-2}$. Thus, the energies have no other dependence on the density but the power law $E \propto \lambda^{-m} \propto \rho^{m/2}$. In 2D linear elasticity, the density is $\propto (1 - \varepsilon^{bg}_{xx} - \varepsilon^{bg}_{yy})$ and then the scaling law tells us that the dependence of $E^{\rm co}(\varepsilon^{bg}_{ij})$ on $(\varepsilon^{bg}_{xx} + \varepsilon^{bg}_{yy})$ is in the form $\propto (1 - \varepsilon^{bg}_{xx} - \varepsilon^{bg}_{yy})^{m/2}$, while the dependencies on $(\varepsilon^{bg}_{xx} - \varepsilon^{bg}_{yy})$ and on $\varepsilon^{bg}_{xy}$ are not known, in principle. We can write this as

$$E^{\rm co}\left(\varepsilon^{bg}_{ij}\right) = \left[1 - \varepsilon^{bg}_{xx} - \varepsilon^{bg}_{yy}\right]^{m/2} G^{\rm co}\left(\varepsilon^{bg}_{xx} - \varepsilon^{bg}_{yy}, \varepsilon^{bg}_{xy}\right), \tag{27}$$

where $G^{\rm co}$ is a function of the deviatoric deformations $\varepsilon^{bg}_{xy}$ and $(\varepsilon^{bg}_{xx} - \varepsilon^{bg}_{yy})$ which change the shape but not the size of the crystal. If the core energy depends also on derivatives of $\varepsilon^{bg}_{ij}$, i.e., if $E^{\rm co} = E^{\rm co}(\varepsilon^{bg}_{ij},\ \partial_k\varepsilon^{bg}_{ij}, \dots)$, we have $G^{\rm co} = G^{\rm co}(\varepsilon^{bg}_{xx} - \varepsilon^{bg}_{yy},\ \varepsilon^{bg}_{xy},\ \partial_k\varepsilon^{bg}_{ij}, \dots)$.

By taking derivatives of Eq. (27) with respect to $\varepsilon^{bg}_{xx}$ and $\varepsilon^{bg}_{yy}$, it is easy to show that

$$-\frac{1}{m}\left[\left.\frac{\partial E^{\rm co}}{\partial\varepsilon^{bg}_{xx}}\right|_{\varepsilon^{bg}_{ij}=0} + \left.\frac{\partial E^{\rm co}}{\partial\varepsilon^{bg}_{yy}}\right|_{\varepsilon^{bg}_{ij}=0}\right] = G^{\rm co}(0,0) = E^{\rm co}(0). \tag{28}$$

Therefore, by relating the derivatives of $E^{\rm co}$ in Eq. (22) with the coefficients in Eq. (3), the scaling law (28) tells us that the core energy at zero background deformations is

$$E^{\rm co} = \frac{1}{m}(M_{xx} + M_{yy}) \tag{29}$$

for systems with power-law interparticle interactions $\propto 1/r^m$. With the results for $M_{xx}$ and $M_{yy}$ obtained from simulations in Sec. IV, we find $E^{\rm co} \approx 0.23\mu a_0^2 \approx 12U_0$ for the system with $V_p(r) = U_0(a_0/r)^{12}$ and density $\rho = 2/(\sqrt{3}a_0^2)$. A definite value for the core energy can be used, e.g., to obtain

TABLE I. Here we list some theoretical approaches that are commented in Sec. V and predict forces on the dislocations that go beyond the PK force: Nonlinear elasticity [56], nonlocal elasticity [28], the strain gradient theory (SGT) of Sec. V A 1 and the core field [34] approaches that result in in Eqs. (15) and (21), respectively, and the core-energy approach of Eq. (22) that can consider the standard core energy shown in Eq. (26), as done in [35], or simply a definite *ad hoc* core energy. In Sec. IV, we observe through simulations that a correction to the PK force is needed in order to explain the results. Properties of this correction, such as linearity, locality, symmetry under Burgers vector inversion, uniqueness, and driving effectiveness were analyzed and quantitative measures of the force were made. In this table, we compare the theoretical approaches with the results of our simulations, indicating if these theories satisfy the properties and are quantitatively correct.

| Validity of some theoretical approaches for predicting a correction to the PK force and its properties | | | | | | |
|---|---|---|---|---|---|---|
| Theoretical approach | Linearity | Locality | Symmetry | Uniqueness | Effectiveness | Quantitative |
| Nonlinear elasticity [56] | no | yes | no | yes | no | |
| Nonlocal elasticity [28] | yes | no | no | yes | no | |
| SGT [Eq. (15)] | yes | yes | no | yes | no | |
| Core field [Eq. (21)] | yes | yes | yes | yes | possibly | no |
| Standard core energy [Eqs. (22) and (26)] | yes | yes | yes | no | no | |
| *Ad hoc* core energy [Eq. (22)] | yes | yes | yes | yes | yes | yes |

the appropriate core radius through Eq. (26) and predict the melting temperature in 2D, through the KTHNY theory [36].

### C. Summary of the agreements and disagreements between the theories and our 2D simulated system

In the previous subsections, we presented some theoretical approaches developed with the aim of providing a correction to the PK force, i.e, the core force. We analyzed if these theories are in agreement with the results of our simulations. Special attention was paid to the physical properties revealed in our simulations, i.e., linearity, locality, symmetry under Burgers vector inversion, uniqueness, and effectiveness to drive a dislocation. When possible, quantitative comparisons concerning the core force values were also made.

In this section, we introduce Table I in order to present a summary of the comparisons made between the different theories and the results of our simulations. These theories are listed along the first column, the properties are listed from the second to the sixth columns, while the last column refers to the quantitative prediction of the core force (see Table I). For instance, if a given theory obeys a certain property, we signal the table with a "yes" and in the opposite case, we signal it with a "no."

If a theory does not satisfy a property such as linearity, locality, symmetry, or uniqueness, it cannot be the core force observed in our system. Consequently, it does not satisfy the property of effectiveness in our simulations and we cannot make a quantitative investigation about it. The noneffectiveness can be due to several reasons. For instance, nonlinear elasticity is expected *a priori* to be noneffective here since it presumes high deformations for the nonlinear effects to be present, which is not the case in our simulations. In contrast, the assumptions for the SGT that resulted in Eq. (15) expect that it would be present in our simulations, but our results showed no such force since this theory does not satisfy the symmetry that we observed.

The nonlinear elasticity theory of [56] presumes high deformations in the system. Our simulations used small background strains and, as expected *a priori*, the linear response of the core force was observed. In addition to nonlinearity, the antisymmetry under **b** inversion is also predicted by this theory and was not observed. Thus, such theory is not effective in our case and we could not quantitatively investigate it. But, it can be relevant in simulations with high deformations.

The nonlocal elasticity theory of [28] predicts nonlocal effects in the force when the background strains have high variations within the region around the dislocation. Our simulations have such type of background strain variations, as it can be seen in Fig. 4, but all the effects observed can be explained locally. In other words, we do not need to know the background strains and their derivatives at other positions but only at the dislocation position. In addition to nonlocality, the antisymmetry under **b** inversion is also predicted by the nonlocal theory and was not observed in our simulations. Thus, such theory is not effective in our case and we could not quantitatively investigate it. Although unlikely, this theory may be relevant in simulations with other crystals or in 3D.

The results of our simulations are compatible with a force that is linearly proportional to local values of the background strain gradients. This is satisfied by the strain gradient theory (SGT) commented in Sec. V A 1 that results in Eq. (15). But, as we can see directly from the equation, it does not obey the symmetry under Burgers vector inversion that is observed in our simulations. Thus, such theory is not effective in our case and we could not quantitatively investigate it. Although unlikely, this theory may be relevant in simulations with other crystals or in 3D.

It is easy to show that the core-field approach, addressed in Sec. V A 2, and used in [34], does satisfy some properties (that is, linearity, locality, symmetry, and uniqueness) of the core force observed in our simulations. This approach also predicts that the values of the coefficients of the core force ($M_{xx}$, $M_{yy}$, ...) are equal to the values of the coefficients of the core field ($M_1$, $M_2$, ...). The latter can be calculated through fittings of the crystal's deformations with the theoretical ones. We perform such fittings in Fig. S2 of the Supplemental Material [49] and observe that the fitted value for $(M_2 - M_1)/2$ depends on the fitting region and does not match with $(M_{xx} - M_{yy})/2$ in any meaningful case. Thus, the core-field approach prediction is not quantitatively satisfactory. It may possibly have some effectiveness in our system, i.e., either it is wrong or it is true and other types of correction are needed to complement it.

Equation (22) gives an approach to obtain the core force through a given core energy, which is taken as a function of the background strains and their derivatives. This approach straightforwardly satisfies the linearity, locality, and symmetry properties. If we consider an *ad hoc* core energy which is unique and gives a core force that quantitatively matches the simulational results, then such approach satisfies all the properties of Table I. This is the ultimate theoretical way to describe the core force observed in our simulations. The remaining question is if the *ad hoc* core energy can be evaluated through other methods. Otherwise, we could not predict the core-force coefficients without directly measuring them.

The standard way to evaluate the core energy is the one of Eq. (26), but it has ambiguity in the choice of the core radius. Thus, such standard core energy (that was used in [35]) does not satisfy the uniqueness property and then cannot be effective and quantified in our system, which observed a unique core force.

## VI. CONCLUSIONS

The effect of strain gradients acting as a driving force on edge dislocations, the so-called core force, was directly observed and quantified. This was done in a system where the strains are known and controllable, using 2D atomistic simulations with periodic boundary conditions. We simulate an idealized model which is able to probe each of the relevant properties of the driving force and then allows us to predict the behavior of the core force in any realistic situation.

Our results confirm that the core force satisfies the properties of effective driving action, linearity, uniqueness, locality, and symmetry under Burgers vector inversion. In order to probe the linearity and locality, our system used strongly varying strains. In such system, we observe that terms with higher-order gradients of strains are necessary to be considered in the core force for a better match with the data.

We compare the observed properties and the measured coefficients of the core force with some theoretical predictions. None of the proposed theories present in the literature were found to be completely satisfactory for explaining the results observed in our 2D system, as summarized in Table I. For instance, the approaches proposed in [35] and in [34] have problems with uniqueness and quantitative predictions, respectively.

In general, the results are compatible with a core force that is originated from a dislocation core energy that depends on the background strains. But, the correct way to measure such energy (and then predict the core-force coefficients) is yet to be discovered. We show that we can go the other way (i.e., to use the results for the core force to evaluate the core energy) in systems with power-law interactions. This is the case in our simulations, with which we obtain $E^{\mathrm{co}} \approx 12U_0$ for a system with $V_p(r) = U_0(a_0/r)^{12}$ and density $\rho = 2/(\sqrt{3}a_0^2)$.

On the theoretical side, we used the core-force analysis to exclude, constrain, improve, or relate some fundamental theories about dislocation dynamics. Moreover, it provides that dislocation distributions have nonreciprocal interactions, serving as a natural model for research on this type of interaction [44,45]. The consideration of the core force can help our understanding of how geometrically necessary dislocations [59] are influenced by strain gradients and then improve phenomenological strain gradient plasticity theories. Potential applications are in studying phenomena that appear in some systems with high strain gradients. These have been better investigated recently and include systems with shock loadings [24], crack tips [60], flexoelectric polarization [61], and deformations at micron and submicron scales (e.g., cutting [62], indentation [63], and torsion [64]), that is, systems with higher and higher strain gradients.

Finally, strain gradient effects on the properties of the solids have gained much attention experimentally [24,65–69] and we hope that their influence on dislocation dynamics can be directly seen in experiments soon.

## ACKNOWLEDGMENTS

We thank R. M. Menezes and E. O. Lima for technical support and E. Clouet for communicating about the core-field approach. We would also like to thank the Coordenação de Aperfeiçoamento de Pessoal de Nível Superior (CAPES) and the Conselho Nacional de Desenvolvimento Científico e Tecnológico (CNPq), Grant No. 140948/2018-0, for the financial support.

[1] V. Volterra, Ann. Éc. Norm. Sup. **24**, 400 (1907).
[2] G. I. Taylor, Proc. R. Soc. London A **145**, 362 (1934).
[3] F. Frank, Adv. Phys. **1**, 91 (1952).
[4] J. P. Hirth and J. Lothe, *Theory of Dislocations* (Wiley, New York, 1982).
[5] L. Kubin, *Dislocations, Mesoscale Simulations and Plastic Flow* (Oxford University Press, Oxford, 2013).
[6] W. L. Bragg and J. F. Nye, Proc. R. Soc. London A **190**, 474 (1947).
[7] Berend van der Meer, W. Qi, R. G. Fokkink, J. Van Der Gucht, M. Dijkstra, and J. Sprakel, Proc. Natl. Acad. Sci. USA **111**, 15356 (2014).
[8] V. Nosenko, G. E. Morfill, and P. Rosakis, Phys. Rev. Lett. **106**, 155002 (2011).
[9] M. C. Miguel and S. Zapperi, Nat. Mater. **2**, 477 (2003).
[10] M. Peach and J. S. Koehler, Phys. Rev. **80**, 436 (1950).
[11] R. Peierls, Proc. Phys. Soc. **52**, 34 (1940).
[12] F. R. N. Nabarro, Proc. Phys. Soc. **59**, 256 (1947).
[13] R. Phillips, *Crystals, Defects and Microstructures: Modeling Across Scales* (Cambridge University Press, Cambridge, 2001).
[14] V. Bulatov and W. Cai, *Computer Simulations of Dislocations* (Oxford University Press, New York, 2006).
[15] J. R. Greer and J. T. D. Hosson, Prog. Mater. Sci. **56**, 654 (2011).
[16] O. Kraft, P. A. Gruber, R. Mnig, and D. Weygand, Annu. Rev. Mater. Res. **40**, 293 (2010).
[17] Y. Gao and H. Bei, Prog. Mater. Sci. **82**, 118 (2016).
[18] G. Z. Voyiadjis and M. Yaghoobi, Crystals **7**, 321 (2017).
[19] G. Z. Voyiadjis and M. Yaghoobi, *Size Effects in Plasticity: From Macro to Nano* (Academic, New York, 2019).

[20] M. Meyers, H. Jarmakani, E. Bringa, and B. Remington, in *Dislocations in Solids*, edited by J. Hirth and L. Kubin (Elsevier, New York, 2009), Vol. 15, p. 91.

[21] B. A. Remington, R. E. Rudd, and J. S. Wark, Phys. Plasmas **22**, 090501 (2015).

[22] L. A. Zepeda-Ruiz, A. Stukowski, T. Oppelstrup, and V. V. Bulatov, Nature (London) **550**, 492 (2017).

[23] C. E. Wehrenberg, D. McGonegle, C. Bolme, A. Higginbotham, A. Lazicki, H. J. Lee, B. Nagler, H.-S. Park, B. A. Remington, R. E. Rudd *et al.*, Nature (London) **550**, 496 (2017).

[24] M. Sliwa, D. McGonegle, C. Wehrenberg, C. A. Bolme, P. G. Heighway, A. Higginbotham, A. Lazicki, H. J. Lee, B. Nagler, H. S. Park, R. E. Rudd, M. J. Suggit, D. Swift, F. Tavella, L. Zepeda-Ruiz, B. A. Remington, and J. S. Wark, Phys. Rev. Lett. **120**, 265502 (2018).

[25] A. Mishra, C. Kunka, M. J. Echeverria, R. Dingreville, and A. M. Dongare, Sci. Rep. **11**, 9872 (2021).

[26] B. Gurrutxaga-Lerma, and M. Simul, Mater. Sci. Eng. **24**, 065006 (2016).

[27] A. C. Eringen, *Nonlocal Continuum Field Theories* (Springer, New York, 2002).

[28] M. Lazar, in *Mechanics of Material Forces*, edited by P. Steinmann and G. A. Maugin (Springer, Boston, 2005), p. 149.

[29] E. C. Aifantis, Int. J. Eng. Sci. **30**, 1279 (1992).

[30] N. Fleck and J. Hutchinson, Adv. Appl. Mech. **33**, 296 (1997).

[31] Y. Huang, S. Qu, K. Hwang, M. Li, and H. Gao, Int. J. Plast. **20**, 753 (2004).

[32] N. A. Fleck, J. W. Hutchinson, and J. R. Willis, J. Appl. Mech. **82**, 071002 (2015).

[33] G. Z. Voyiadjis and Y. Song, Int. J. Plast. **121**, 21 (2019).

[34] E. Clouet, Phys. Rev. B **84**, 224111 (2011).

[35] M. Iyer, B. Radhakrishnan, and V. Gavini, J. Mech. Phys. Solids **76**, 260 (2015).

[36] K. J. Strandburg, Rev. Mod. Phys. **60**, 161 (1988).

[37] B. Gurrutxaga-Lerma and J. Verschueren, Phys. Rev. Materials **3**, 113801 (2019).

[38] S. Das and V. Gavini, J. Mech. Phys. Solids **104**, 115 (2017).

[39] Y. Hu, B. Szajewski, D. Rodney, and W. Curtin, Modell. Simul. Mater. Sci. Eng. **28**, 015005 (2020).

[40] M. Zaiser and S. Sandfeld, and M. Simul, Mater. Sci. Eng. **22**, 065012 (2014).

[41] C. H. Henager and R. G. Hoagland, Scr. Mater. **50**, 1091 (2004).

[42] N. Irani, Y. Murugesan, C. Ayas, and L. Nicola, Mech. Mater. **165**, 104137 (2022).

[43] O. S. Vaulina, I. I. Lisina, and E. A. Lisin, J. Exp. Theor. Phys. **121**, 717 (2015).

[44] S. A. M. Loos and S. H. L. Klapp, New J. Phys. **22**, 123051 (2020).

[45] L. Braverman, C. Scheibner, B. VanSaders, and V. Vitelli, Phys. Rev. Lett. **127**, 268001 (2021).

[46] A. Poncet and D. Bartolo, Phys. Rev. Lett. **128**, 048002 (2022).

[47] B. VanSaders, J. Dshemuchadse, and S. C. Glotzer, Phys. Rev. Materials **2**, 063604 (2018).

[48] S. C. Kapfer and W. Krauth, Phys. Rev. Lett. **114**, 035702 (2015).

[49] See Supplemental Material at http://link.aps.org/supplemental/10.1103/PhysRevB.106.224105 for more details. See Secs. II and III of the Supplemental Material for a detailed derivation of Eq. (10). See Sec. IV of the Supplemental Material for a detailed derivation of the Peach-Koehler force and its correction in a particular strain gradient theory of elasticity, where a term like $-C^{(1)}_{ijklm}\varepsilon_{ij}\partial_m\varepsilon_{kl}/2$ is added inside the integral of Eq. (7). See Sec. V of the Supplemental Material for details on the simulational analysis that we made about the core field in our system.

[50] S. A. Khrapak, N. P. Kryuchkov, and S. O. Yurchenko, Phys. Rev. E **97**, 022616 (2018).

[51] X. Zhou, D. Ward, J. Zimmerman, J. Cruz-Campa, D. Zubia, J. Martin, and F. van Swol, J. Mech. Phys. Solids **91**, 265 (2016).

[52] X. W. Zhou, R. B. Sills, D. K. Ward, and R. A. Karnesky, Phys. Rev. B **95**, 054112 (2017).

[53] A. Satoh, *Introduction to Practice of Molecular Simulation: Molecular Dynamics, Monte Carlo, Brownian Dynamics, Lattice Boltzmann and Dissipative Particle Dynamics* (Elsevier, Amsterdam, 2011).

[54] M. Lazar and H. O. K. Kirchner, Int. J. Solids Struct. **44**, 2477 (2007).

[55] G. Po, M. Lazar, N. C. Admal, and N. Ghoniem, Int. J. Plast. **103**, 1 (2018).

[56] P. Steinmann, J. Mech. Phys. Solids **50**, 1743 (2002).

[57] The condition for Eq. (26) to converge can be used to measure $K$, as $E^{\mathrm{co,\,std}}(R)$ diverges logarithmically for a wrong value of $K$. The convergence becomes significantly fast after some point, which can be of the order of $R \sim 10b$ [35]. But a formal definition of the standard core energy would need to take the limit $R \to \infty$ since there is no finite $R$ above which the Volterra strains are exactly equal to the real crystal ones. In fact, the core-field approach [34], discussed more in Sec. V A 2, predicts strains and energy corrections to Volterra that decay, respectively, as $1/r^2$ and $1/R^2$.

[58] L. Pizzagalli, J.-L. Demenet, and J. Rabier, Phys. Rev. B **79**, 045203 (2009).

[59] M. Montagnat, P. Duval, P. Bastie, and B. Hamelin, Scr. Mater. **49**, 411 (2003).

[60] V. N. Shlyannikov, A. V. Tumanov, and R. M. Khamidullin, Phys. Mesomech. **24**, 257 (2021).

[61] Y. Liu, X. Cui, R. Niu, S. Zhang, X. Liao, S. D. Moss, P. Finkel, M. Garbrecht, S. P. Ringer, and J. M. Cairney, Nat. Commun. **13**, 335 (2022).

[62] M. Demiral, A. Roy, and V. V. Silberschmidt, J. Manuf. Process. **74**, 511 (2022).

[63] T. Bond, A. Badmos, R. A. Ahmed, J. D. Obayemi, A. Salifu, and N. Rahbar, and W. O. Soboyejo, Mater. Sci. Eng. A **839**, 142542 (2022).

[64] J. K. Han, X. Liu, I. Lee, Y. O. Kuzminova, S. A. Evlashin, K. D. Liss, and M. Kawasaki, Mater. Lett. **302**, 130364 (2021).

[65] B. Rozaliya and I. Gene, *Strain and Dislocation Gradients from Diffraction. Spatially Resolved Local Structure and Defects* (Imperial College Press, London, 2014).

[66] Y. L. Tang, Y. L. Zhu, Y. Liu, Y. J. Wang, and X. L. Ma, Nat. Commun. **8**, 15994 (2017).

[67] B. Wang, Y. Gu, S. Zhang, and L.-Q. Chen, Prog. Mater. Sci. **106**, 100570 (2019).

[68] M. Goldsche, J. Sonntag, T. Khodkov, G. J. Verbiest, S. Reichardt, C. Neumann, T. Ouaj, N. von den Driesch, D. Buca, and C. Stampfer, Nano Lett. **18**, 1707 (2018).

[69] O. Gorobtsov and A. Singer, J. Synchrotron Rad. **29**, 866 (2022).